

High-Precision Heading Control of an Autonomous Sailboat: a Robust Nonlinear Approach

Sean Smith¹, *Student Member, IEEE*, Emmanuel Witrant¹, and Ya-Jun Pan², *Senior Member, IEEE*

Abstract—This article investigates high-precision robust heading control for an autonomous sailboat. First, the mathematical model of an autonomous sailboat is highlighted and discussed, with a particular focus on the heading dynamics that must be robustly controlled under real-world conditions. Typical control difficulties such as system disturbances, modeling uncertainty, control actuation saturation, and measurement noise are considered and addressed with reference to the controller and system modeling. We propose a control method that ensures robust heading control of an autonomous sailboat in the presence of these challenges. A reference simulator in Matlab/Simulink is used as a simulation testbed to demonstrate the benefits of state-of-the-art robust control developments. A multiphase simulation is conducted to compare the advantages and disadvantages of model-based robust control with linear techniques such as proportional-integral-derivative (PID) control.

Index Terms—Autonomous sailboat, sailboat modelling, robust control.

I. INTRODUCTION

An unmanned autonomous sailboat is a robotic vessel that harnesses wind energy for propulsion while autonomously controlling its sails and steering. This system has emerged to offer an environmentally friendly solution to transportation challenges, compared to traditional marine vehicles. The sailboat can operate in a wide range of conditions and sail for extended periods of time across large bodies of water [1]. Additionally, the sailboat is playing a vital function in monitoring challenges, including ocean sampling and surveying [2], and marine environment and biogeochemistry monitoring [3], [4].

The utilization of wind-based propulsion introduces mathematical complexities into the modelling process due to the unpredictability of marine environments [5], and the nature of aerodynamic forces. Typical four-degrees-of-freedom (4-DOF) models include surge, sway, roll, and yaw motions [6]. Modeling these motions results in a dynamic system that is highly coupled, complex, nonlinear, and nonaffine, making it challenging to design explicit model-based controllers that

stabilize the nonlinear dynamics. Additionally, one must consider the influence of real-world conditions such as system disturbances, modelling uncertainty, and measurement noise.

Due to the uncertainty and complexity of the ocean environment, accurately modeling the sailboat and the forces acting on it is challenging. However, analogous to Fossen's marine vehicle modelling methods [6], Xiao and Jouffroy [7] first developed a nonlinear 4-DOF model for a sailboat containing a sail, rudder, keel and hull, and the forces and moments acting on each component. They also introduced a backstepping control approach. Along with the modelling, a reference simulator was provided as an open-source learning tool for researchers in sailboat modelling and control [8]. The modelling and simulator has laid the groundwork for extensive research, literature, and contributions in autonomous sailboat robotics. The simulator is used to outline the control characteristics discussed in this paper.

Motivated by the above discussion, this paper aims to provide a general overview of applying robust control to an autonomous sailboat system. It highlights the benefits of state-of-the-art control strategies, including fast convergence, disturbance handling, adaptive gain selection, noise sensitivity, chatter attenuation, control saturation handling, and feedforward control. Additionally, comparisons are made with classical control techniques such as PID control. A simulator in Matlab/Simulink, implementing a 4-DOF sailboat model [6], [7], is used to conduct dynamic tracking maneuvers for multiphase heading, demonstrating the benefits of robust control techniques.

II. MODELLING

Consider the 4-DOF radio-controlled sailboat DragonFlite 95 V2, built by Joysway[®], depicted in Fig. 1. The unit vectors on the DragonFlite $[\vec{b}_x, \vec{b}_y, \vec{b}_z] \in SO(3)$ are located at the center of gravity (CG) and make the body-fixed reference frame, which is a rotating reference frame attached to the sailboat. Additionally, the north-east-down (NED) coordinate system $\{\vec{i}_x, \vec{i}_y, \vec{i}_z\}$ represents the inertial frame.

The kinematics of the sailboat are represented by [7]

$$\begin{cases} \dot{x} &= u \cos(\psi) - v \cos(\phi) \sin(\psi) \\ \dot{y} &= u \sin(\psi) + v \cos(\phi) \cos(\psi) \\ \dot{\phi} &= p \\ \dot{\psi} &= r \cos(\phi), \end{cases} \quad (1)$$

where $\eta = [x, y, \phi, \psi]^T$ represents the boat's position, roll, and yaw in the inertial frame, and $\nu = [u, v, p, r]^T$ denotes the

Thanks to the Natural Sciences and Engineering Research Council (NSERC) of Canada, France Canada Research Fund (FCRF), and Conseil National des Universités for supporting this work.

¹ S. Smith and E. Witrant are with the GIPSA-lab, Université Grenoble Alpes - CNRS, F-38000, Grenoble, France, and the Department of Mechanical Engineering, Dalhousie University, Halifax NS B3H 4R2, Canada (e-mails: s.smith@dal.ca, emmanuel.witrant@univ-grenoble-alpes.fr).

² Ya-Jun Pan is with the Advanced Control and Mechatronics Laboratory, Department of Mechanical Engineering, Dalhousie University, Halifax NS B3H 4R2, Canada (e-mail: ya.jun.pan@dal.ca).

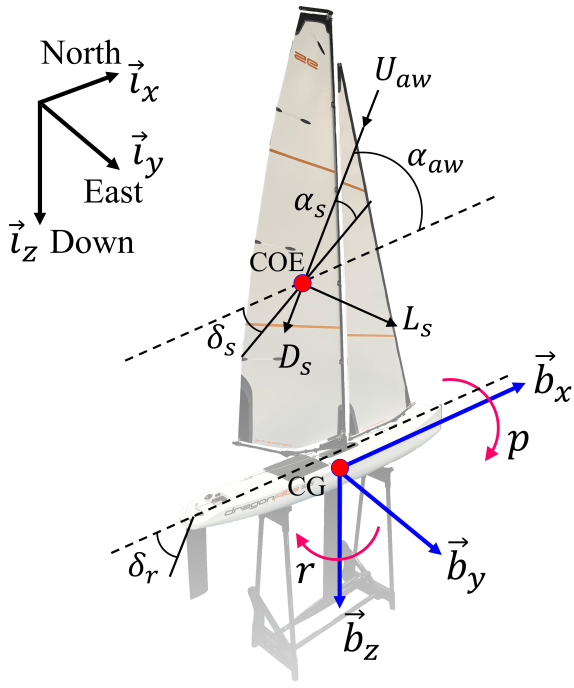


Fig. 1: Sailboat body-fixed coordinate frame $\{\vec{b}_x, \vec{b}_y, \vec{b}_z\}$ with a North-East-Down inertial reference frame $\{\vec{i}_x, \vec{i}_y, \vec{i}_z\}$, illustrated on a Joysway® DragonFlite 95 V2.

generalized velocity vector containing the linear and angular velocities in the body frame. The kinetics are represented in (2), where F_{xi} and F_{yi} represent the forces along the surge and sway imposed by the sail, rudder, hull and keel, denoted respectively by $i \in \{s, r, h, k\}$. The disturbing forces are given as F_{wu} and F_{wv} . The remaining moments are labelled analogously. The terms $a, b, c,$ and d are proportional constants of the restoring forces that direct the sailboat to equilibrium, m is the total mass of the boat, I_{xx} and I_{zz} are the moments of inertia around surge and heave, and $X_{\dot{u}}, Y_{\dot{v}}, K_{\dot{p}},$ and $N_{\dot{r}}$ are the added mass coefficients in the body frame.

The aerohydrodynamics for a foil in a fluid are used to estimate the forces and moments acting on each component of the sailboat. Using thin airfoil theory, the lift and drag are given as

$$\begin{cases} L &= \frac{1}{2}\rho AU_a^2 C_L(\alpha) \\ D &= \frac{1}{2}\rho AU_a^2 C_D(\alpha), \end{cases} \quad (3)$$

where α is the angle of attack between the apparent incoming flow and the foil, C_L and C_D are the lift and drag coefficients

that are functions of α , U_a is the apparent wind speed, and A represents the plan area of the foil.

The wind dynamics on the sail are assumed to act through a single point on the foil, which is referred to as the aerodynamic center of effort (COE). This interaction generates the boat's surge propulsion. The speed interaction between the sailboat and wind is described by the apparent wind speed U_{aw} and bearing angle α_{aw} , which are related to the true wind speed U_{tw} and true wind angle α_{tw} as [7]

$$\begin{cases} U_{awu} &= U_{tw} \cos(\alpha_{tw} - \psi) - u + ry_s \\ U_{awv} &= U_{tw} \sin(\alpha_{tw} - \psi) \cos(\phi) - v - rx_s + pz_s \\ \alpha_{aw} &= -\arctan\left(\frac{U_{awv}}{U_{awu}}\right) + 90^\circ \text{sign}\left(\frac{U_{awv}}{U_{awu}}\right) \\ &\quad + 90^\circ \text{sign}(U_{awv}), \end{cases} \quad (4)$$

where the resulting apparent wind speed is $U_{aw} = \sqrt{U_{awu}^2 + U_{awv}^2}$, and x_s, y_s and z_s are the coordinates of the COE in the body frame. The resulting angle of attack for the sail is $\alpha_s = \alpha_{aw} - \delta_s$, where δ_s is the sail angle in the body frame. Using (3) and the geometric relation between the COE and CG, the forces F_{xs}, F_{ys} , and moments M_{xs}, M_{zs} are expressed as

$$\begin{cases} F_{xs} &= L_s \sin(\alpha_{aw}) - D_s \cos(\alpha_{aw}) \\ F_{ys} &= L_s \cos(\alpha_{aw}) + D_s \sin(\alpha_{aw}) \\ M_{xs} &= F_{ys} |z_s| \\ M_{zs} &= F_{ys} (x_m - x_{sm} \cos(\delta_s)) - F_{xs} x_{sm} \sin(\delta_s), \end{cases} \quad (5)$$

where x_{sm} is the distance between the mast and sail's COE, and x_m represents the x -coordinate of the mast in the body frame. The same process can be followed to determine the kinetics of the rudder, hull, and keel analogously. Specifically, the turning moment produced by the rudder actuator is derived as

$$M_{zr} = -(L_r \cos(\alpha_{ar}) + D_r \sin(\alpha_{ar})) |x_r|, \quad (6)$$

where α_{ar} is the apparent rudder angle, with the rudder angle given as $\alpha_r = \alpha_{ar} - \delta_r$. Assuming no currents, the true water speed is zero. Additionally, (6) can be further simplified by assuming that the apparent angle of the water on the rudder is very small $\alpha_{ar} \approx 0$, as done in [7]. This assumption negates the drag on the rudder, making the apparent water speed at the stern equal to the sailboat's speed. The resulting angle of attack of water on the rudder is given by $\alpha_r = -\delta_r$. Finally, using (6) and (3) yields

$$\hat{M}_{zr} = -\frac{1}{2}\rho_w A_r U_{ar}^2 |x_r| C_{Lr}(-\delta_r), \quad (7)$$

where ρ_w is the water density, A_r is the plan area of the rudder, x_r is the x -coordinate of the rudder's centroid in the body

$$\begin{cases} (m - X_{\dot{u}})\dot{u} &= F_{xs} + F_{xr} + (m - Y_{\dot{v}})vr - F_{xk} - F_{xh} + F_{wu} \\ (m - Y_{\dot{v}})\dot{v} &= F_{ys} + F_{yr} - (m - X_{\dot{u}})ur - F_{yk} - F_{yh} + F_{wv} \\ (I_{xx} - K_{\dot{p}})\dot{p} &= M_{xs} + M_{xr} - c|p|p - a\phi^2 - b\phi - M_{xk} - M_{xh} + M_{wp} \\ (I_{zz} - N_{\dot{r}})\dot{r} &= M_{zs} + M_{zr} - (X_{\dot{u}} - Y_{\dot{v}})uv - d|r|r \cos(\phi) - M_{zk} - M_{zh} + M_{wr}, \end{cases} \quad (2)$$

frame, $U_{ar} = \sqrt{u^2 + v^2}$, and $C_{Lr}(-\delta_r)$ is the lift coefficient, which is a function of the rudder angle. More details on the sailboat modelling can be found in [7].

Analyzing the DragonFlite in Fig. 1, it is clear that the sail's plan area is much larger than that of the rudder. This makes the sail the dominant control actuator in the surge, sway, and roll equations of (2). Common methods for handling the sail angle include polar diagrams [9], or extremum seeking [10], [11] and speed optimization methods to maximize the sailboat's speed under various wind directions. With the mast centrally positioned and the heavy keel and internal electronics placing the CG directly under the mast, there is minimal displacement between the CG and COE. Consequently, the rudder, being far from the CG along the sail length, is the dominant actuator for the sailboat's heading dynamics. Therefore, by decoupling the sail actuator from the heading dynamics, the control objective is to design a control law for δ_r to have the sailboat heading ψ track a desired reference heading ψ_r in the presence of disturbances, onboard measurement noise, and limited control actuation.

III. HEADING CONTROL ARCHITECTURE

The basic premise of heading control is to minimize the heading error between the current sailboat heading ψ and the reference heading ψ_r generated by a guidance system. This can be accomplished through a variety control methods [12]. However, in the presence of external disturbances, unmodeled aerohydrodynamics, input saturation, and measurement noise, a robust controller presents a desirable solution to ensure stable reference tracking.

The control architecture for the heading dynamics control of an autonomous sailboat is illustrated in Fig. 2. As shown, the robust controller must provide a control input δ_r , which is saturated based on actuator operating limits δ_r^{sat} . This control input aims to drive the sailboat's heading ψ to track a desired reference heading ψ_r while accounting for system perturbations and onboard measurement noise.

For the controller implementation in the simulations (Section IV), we combine a fast-converging robust control strategy [13] with a robust switching controller designed to attenuate chattering component [14]. This approach includes adaptive gain selection and an anti-windup (AW) compensator method to ensure a stable closed-loop system while limiting the influence of control input saturation. The controller is labeled as: Robust-AW, and is given as

$$M_{zr} = \Pi \left[-\frac{|e_2|^{2-\omega}}{\omega\beta_2} (1 + \beta_1\gamma|e_1|^{\gamma-1}) \text{sign}(e_2) + \frac{1}{\vartheta}\dot{\mu} + \ddot{\psi}_r - \rho(r, \phi, \dot{\phi}) + \xi \right] + \hat{\Upsilon}, \quad (8)$$

where $\Pi = \frac{I_{zz} - N_r}{\cos\phi}$, $e_1 = \psi - \psi_r$, $e_2 = \dot{\psi} - \dot{\psi}_r$, $\beta_1, \beta_2 \in \mathbb{R}^+$, $\vartheta = \beta_2\omega|e_2|^{\omega-1}$, $\rho(r, \phi, \dot{\phi}) = -r\dot{\phi}\sin(\phi)$, $\omega = q/p$, and

the coefficients q and p are positive odd numbers satisfying $1 < \omega < 2$ and $\gamma > q/p$. We then have

$$\begin{cases} \xi &= -k_1|s|^{\frac{1}{2}}\text{sign}(s) + \nu \\ \dot{\nu} &= -k_2\text{sign}(s) \\ \Upsilon &= -M_{zs} + (X_{\dot{u}} - Y_{\dot{v}})uw + d|r|\cos\phi + M_{zk} \\ &\quad + M_{zh} - M_{wr}, \end{cases} \quad (9)$$

where $k_1, k_2 \in \mathbb{R}^+$. Term ξ represents a STA, $\dot{\mu}$ is an auxiliary anti-windup compensator, and $\hat{\Upsilon}$ is a system estimator designed to estimate Υ online. The details for $\dot{\mu}$, $\hat{\Upsilon}$, and adaptive algorithm for k_1, k_2 are omitted from this paper. The robust controller without anti-windup compensation is labelled as: Robust.

IV. SIMULATION STUDIES

To evaluate the control strategies, we conducted simulations in Matlab/Simulink while implementing the differential equation model of the 4-DOF sailboat described in Section II. A 12-m-long keeled sailboat described in [7] was chosen as the physical model. To study the robustness of the control strategies, the sailboat was targeted to track complex heading dynamic trajectories in the presence of real sea conditions, which included aerodynamic force-models and wind-based wave models [6]. The wind consists of a mean speed component, and fluctuating component represented by the NORSOK wind spectrum. The JONSWAP wave spectrum is adapted to replicate the marine wave disturbances. This is approximated by separating the influence of wave-induced disturbances into the first-order wave frequency motion and second-order wave drift forces. More details can be found in [6].

The proposed methods are investigated in breezy conditions categorized by the Beaufort wind scale No. 4 of the North wind, with a mean wind velocity of 6.8 m/s and with a direction of $\alpha_{tw} = \pi\text{ rad}$, as illustrated in Fig. 3(b). Additionally, the control methods are simulated under strong wind conditions with a mean wind velocity of 12 m/s to test their robustness.

In addition to system disturbances, sensor measurement noise is introduced. In a real system, onboard inertial measurement unit (IMU) sensors would send data to the onboard extended Kalman filter (EKF), which fuses measurements from various sensors to estimate the system states (see Fig. 2). To simulate the resulting measurement noise, white noise with a standard deviation of $\sigma = 0.001$ is added to each measurement.

In simulations, Robust-AW discussed in Section III is compared to the backstepping (BS) controller from [7] and a proportional-integral-derivative featuring back-calculation (PID-BC) [15]. Additionally, a standard PID controller without back-calculation, and the Robust controller without anti-windup compensation are simulated to illustrate the integral windup effect in the presence of control saturation.

The mean absolute error (MAE) was used as a tracking performance metric, and the mean absolute control effort

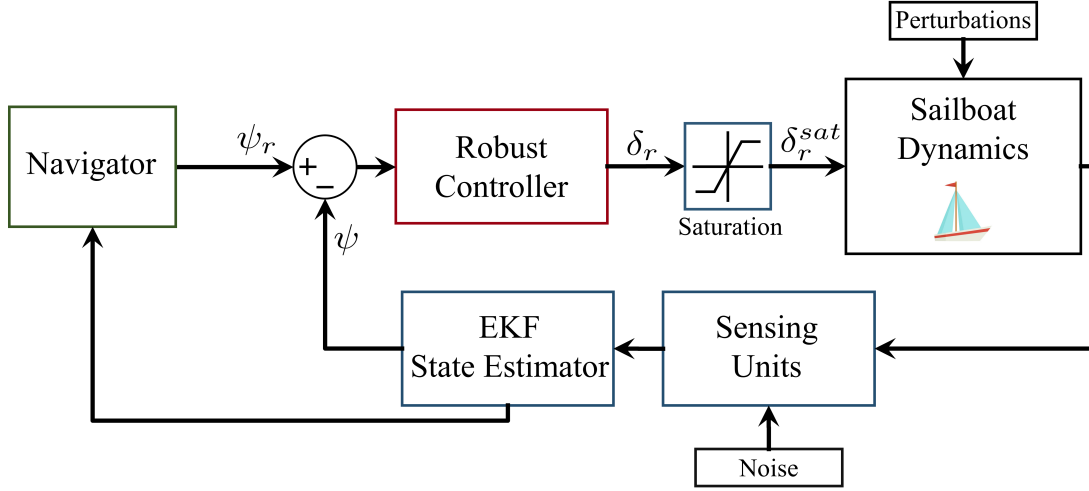


Fig. 2: Guidance, navigation, and control architecture for the heading dynamics of an autonomous sailboat.

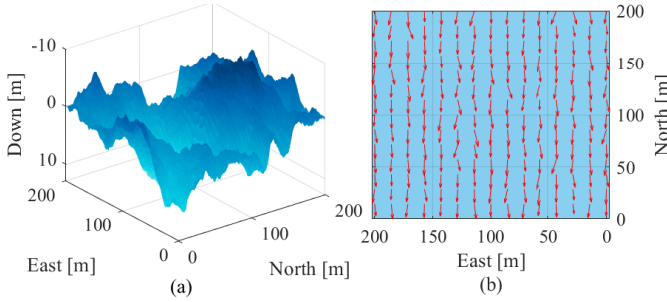


Fig. 3: Matlab simulation disturbance profiles: (a) JONSWAP generated waves; (b) Wind field of the NORSOK spectrum.

(MAC) was used to measure control effort in the simulations. These are calculated as:

$$\text{MAE} = \frac{1}{t_f - t_0} \int_{t_0}^{t_f} |e_1| dt \quad (10)$$

$$\text{MAC} = \frac{1}{t_f - t_0} \int_{t_0}^{t_f} |\delta_r| dt. \quad (11)$$

Remark 1. To ensure a meaningful control comparison, the *PID-BC*, *BS*, and *Robust-AW* controllers were tuned to achieve a tracking performance with a MAE below 1° under non-disturbed conditions.

A. Multi-Phase Matlab/Simulink Simulations

The multi-phase simulation experiment is conducted to highlight the control techniques discussed in Section III. The heading tracking results are shown in Fig. 4, and the performance metrics are quantified in Table I. In *Phase 1*, the focus is on performing a tacking maneuver (the bow of the boat passes through the wind) in calm water conditions ($U_{tw}^{mean} = 6.8 \text{ m/s}$) with control input saturation. In *Phase 2*, the emphasis shifts towards assessing the heading stability while maintaining a constant reference with a crosswind

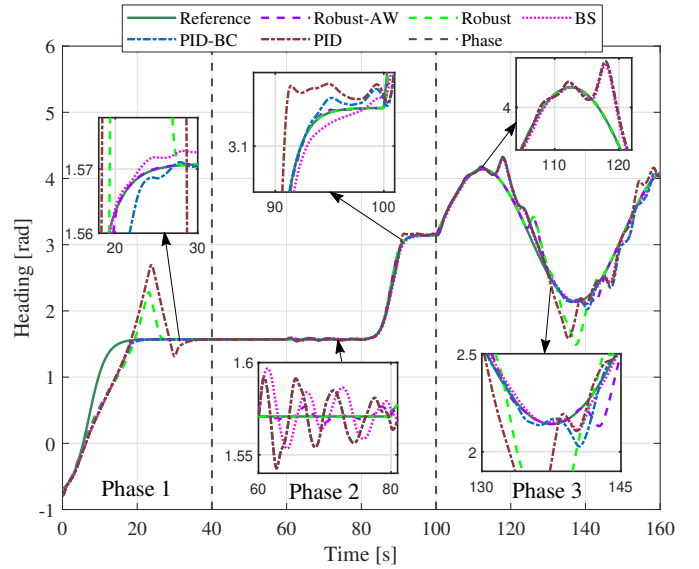


Fig. 4: Multi-Phase simulation heading response profiles under various conditions: Phase 1) Tacking maneuver in calm water conditions; Phase 2) Constant heading reference while introducing rough water conditions at $t = 60 \text{ s}$; Phase 3) Jibing maneuvers in rough water conditions.

direction, in the presence of calm and rough water conditions ($U_{tw}^{mean} = 12 \text{ m/s}$). Finally, *Phase 3* tests the control performance by initiating jibing maneuvers (the stern of the boat passes through the wind) in the presence of rough water conditions.

1) *Phase 1*: During the first phase, the sailboat began with initial conditions $[x, y, \phi, \psi, u, v, p, r]^T(0) = [0, 0, 0, -\pi/4, 3, 0, 0, 0]^T$ and was tasked to tack to a heading angle of $\psi_r = \pi/2 \text{ rad}$ in calm water conditions. The reference heading was represented by a smooth step input to perform the tacking maneuver.

TABLE I: Simulation performance metrics-tracking performance for each controller.

MAE [deg]	Phase 1	Phase 2	Phase 3
PID-BC	7.70	0.60	5.44
PID	16.82	0.88	7.39
BS	7.95	0.89	4.26
Robust-AW	7.40	0.06	1.94
Robust	11.52	0.03	4.81
MAC [rad]	Phase 1	Phase 2	Phase 3
PID-BC	0.224	0.088	0.339
PID	0.387	0.088	0.383
BS	0.223	0.076	0.331
Robust-AW	0.238	0.089	0.288
Robust	0.326	0.084	0.369

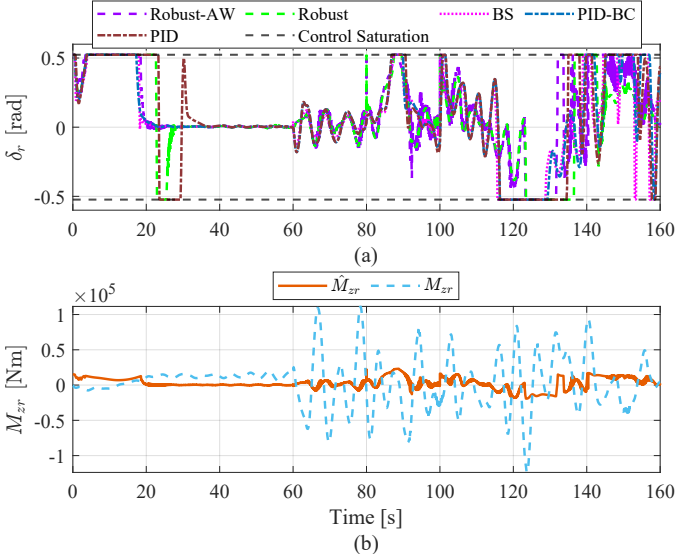


Fig. 5: Matlab simulation response profiles: (a) Control input δ_r for each control algorithm; (b) Turning moment M_{zr} and estimated turning moment \hat{M}_{zr} .

During the tacking maneuver, both the Robust and PID controllers experienced performance instability and overshoot (see Fig. 4) due to the presence of control input saturation. The windup effect increased the MAE and MAC (see Table I), which is illustrated in Fig. 5(a). The anti-windup and back-calculation methods were able to mitigate this issue, with the Robust-AW and PID-BC avoiding the windup instability at $t = 24$ s and reducing the MAE by 43.5% and 74.4% during *Phase 1*, respectively. From Fig. 6(a), the adaptive gains (k_1, k_2) adjusted to ensure a robust and stable controller, while keeping the gain selection at a minimum to reduce sensitivity to input noise and sampling step [16]. The performance of the backstepping controller was on par with that of the Robust-AW and PID-BC controllers, as highlighted in Table I.

2) *Phase 2*: In this phase, the sailboat maintains a constant reference heading of $\psi_r = \pi/2$ rad in crosswind conditions before performing a jibe maneuver to $\psi_r = \pi$ rad, facing directly downwind in the no-go zone. At $t = 60$ s, the calm water conditions transition to rough water conditions with high wind and wave disturbances. Each controller robustly

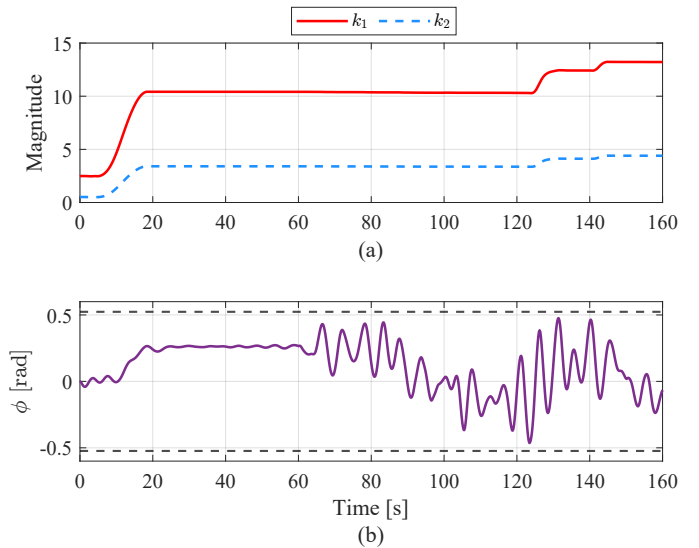


Fig. 6: Matlab simulation response profiles: (a) Time variation of adaptive gains for the Robust-AW simulation; (b) Roll angle response of the 4-DOF sailboat during the Robust-AW simulation.

maintains the reference heading while keeping the MAE below 1° .

After the onset of rough water conditions at $t \geq 60$ s, the Robust-AW controller experiences an increased chattering amplitude due to the perturbation increase, which is directly correlated [17]. The chattering may be mitigated in a variety of ways, including introducing a disturbance observer to estimate and damp the unknown system perturbations [18], reducing the sampling step, or using boundary layer smoothing functions.

The chatter increase is evident in the calculation of \hat{M}_{zr} (see Fig. 5(b)), which is a function of δ_r . The \hat{M}_{zr} turning moment, calculated with δ_r and the modelling assumptions in Section II, is comparable to the true system turning moment M_{zr} during calm water conditions $t < 60$ s. However, in the presence of rough water conditions $t \geq 60$ s, the influence of drag on the turning moment M_{zr} becomes significant (see Fig 5(b)). Consequently, the model uncertainty introduced in the model-based controller design needs to be compensated by the robustness of the control solution.

3) *Phase 3*: The sailboat is tasked with performing jibing maneuvers in the presence of large wave disturbances and control input saturation. Similar to *Phase 1*, the introduction of both control input saturation and system perturbations results in performance deterioration for the Robust and PID controllers due to their struggle with the windup effect. The anti-windup and back-calculation techniques exhibit MAE reductions of 85% and 30.4%, respectively.

The smooth reference ψ_r for $t \in (100, 160)$ s allowed for higher-order feedforward tracking setpoints in ψ_r and $\dot{\psi}_r$ to be used by the Robust controllers, improving performance during the jibing maneuvers. Without velocity and acceleration tracking, the robotic system is likely to lag behind during

complex maneuvers. Higher-order feedforward setpoints are essential for higher-order robust controllers, contributing to the improved performance during *Phase 3*. A similar system could be accomplished by introducing cascade PID controllers, a configuration commonly found in quadcopter control systems [18].

It is found that the roll angle is constrained to less than 30° , which is defined as the stable zone (see Fig. 6(b)). The roll angle reaches a maximum of 26.8° during the jibing maneuvers in rough water conditions. While stable roll dynamics were ensured in this particular simulation, it would be a good practice to integrate a separate roll angle stabilizer [19].

V. CONCLUSION

In line with nautical practices and state-of-the-art control techniques, this paper presents a high-precision robust heading control approach for an autonomous sailboat. Techniques such as fast convergence, chatter attenuation, anti-windup compensation, and noise sensitivity are discussed. Furthermore, an existing simulator, developed for research testing based on a 4-DOF sailboat model, is examined. The simulator serves as an experimental testbed to demonstrate robust control techniques through complex sailboat maneuvers, including tacking, crosswind reference tracking, and jibing, conducted under both calm and rough water conditions. Future work will involve detailing the mathematical aspects of the proposed Robust control solutions and applying the results to the DragonFlite sailboat hardware.

REFERENCES

- [1] Y. An, J. Yu, and J. Zhang, "Autonomous sailboat design: A review from the performance perspective," *Ocean Engineering*, vol. 238, p. 109753, 2021.
- [2] N. A. Cruz and J. C. Alves, "Autonomous sailboats: An emerging technology for ocean sampling and surveillance," in *OCEANS 2008*. IEEE, 2008, pp. 1–6.
- [3] Y.-T. Ang, W.-K. Ng, Y.-W. Chong, J. Wan, S.-Y. Chee, and L. B. Firth, "An autonomous sailboat for environment monitoring," in *2022 Thirteenth International Conference on Ubiquitous and Future Networks (ICUFN)*. IEEE, 2022, pp. 242–246.
- [4] F. Chai, K. S. Johnson, H. Claustre, X. Xing, Y. Wang, E. Boss, S. Riser, K. Fennel, O. Schofield, and A. Sutton, "Monitoring ocean biogeochemistry with autonomous platforms," *Nature Reviews Earth & Environment*, vol. 1, no. 6, pp. 315–326, 2020.
- [5] M. Zyczkowski and R. Szlapczynski, "Collision risk-informed weather routing for sailboats," *Reliability Engineering & System Safety*, vol. 232, p. 109015, 2023.
- [6] T. I. Fossen, "Marine control systems—guidance, navigation, and control of ships, rigs and underwater vehicles," *Marine Cybernetics, Trondheim, Norway, Org. Number NO 985 195 005 MVA*, www.marinecybernetics.com, ISBN: 82 92356 00 2, 2002.
- [7] L. Xiao and J. Jouffroy, "Modeling and nonlinear heading control of sailing yachts," *IEEE Journal of Oceanic engineering*, vol. 39, no. 2, pp. 256–268, 2013.
- [8] J. Jouffroy, "Sailingyachtmodel.zip," <https://www.mathworks.com/matlabcentral/fileexchange/47981-sailingyachtmodel.zip>, July 29 2024, MATLAB Central File Exchange.
- [9] R. Stelzer and T. Pröll, "Autonomous sailboat navigation for short course racing," *Robotics and autonomous systems*, vol. 56, no. 7, pp. 604–614, 2008.
- [10] L. Xiao, J. C. Alves, N. A. Cruz, and J. Jouffroy, "Online speed optimization for sailing yachts using extremum seeking," in *2012 Oceans*. IEEE, 2012, pp. 1–6.
- [11] Z. Shen, X. Fan, H. Yu, C. Guo, and S. Wang, "A novel speed optimisation scheme for unmanned sailboats by sliding mode extremum seeking control without steady-state oscillation," *The Journal of Navigation*, vol. 75, no. 3, pp. 745–762, 2022.
- [12] Y. Tipsuwan, P. Sanposh, and N. Techajaronjit, "Overview and control strategies of autonomous sailboats—a survey," *Ocean Engineering*, vol. 281, p. 114879, 2023.
- [13] L. Yang and J. Yang, "Nonsingular fast terminal sliding-mode control for nonlinear dynamical systems," *International Journal of Robust and Nonlinear Control*, vol. 21, no. 16, pp. 1865–1879, 2011.
- [14] J. A. Moreno and M. Osorio, "Strict lyapunov functions for the super-twisting algorithm," *IEEE Transactions on Automatic Control*, vol. 57, no. 4, pp. 1035–1040, 2012.
- [15] L. R. da Silva, R. C. Flesch, and J. E. Normey-Rico, "Analysis of anti-windup techniques in pid control of processes with measurement noise," *IFAC-PapersOnLine*, vol. 51, no. 4, pp. 948–953, 2018.
- [16] A. Levant, "Higher-order sliding modes, differentiation and output-feedback control," *International journal of Control*, vol. 76, no. 9-10, pp. 924–941, 2003.
- [17] V. K. Tripathi, A. K. Kamath, L. Behera, N. K. Verma, and S. Nahavandi, "Finite-time super twisting sliding mode controller based on higher-order sliding mode observer for real-time trajectory tracking of a quadrotor," *IET Control Theory & Applications*, vol. 14, no. 16, pp. 2359–2371, 2020.
- [18] S. Smith and Y. J. Pan, "Adaptive observer-based super-twisting sliding mode control for low altitude quadcopter grasping," *IEEE/ASME Transactions on Mechatronics*, May 2024, in Press.
- [19] Y. Deng, X. Zhang, Q. Zhang, and Y. Hu, "Event-triggered composite adaptive fuzzy control of sailboat with heeling constraint," *Ocean Engineering*, vol. 211, p. 107627, 2020.